Chapter 5

Accumulation, Storage and Manipulation of Large Numbers of Positrons in Traps II. – Selected Topics[a]

Clifford M. Surko, James R. Danielson and Toby R. Weber

University of California, San Diego,
La Jolla CA 92093, USA
csurko@ucsd.edu; jdan@physics.ucsd.edu; tobyweber@gmail.com

This chapter describes research to create, manipulate and utilize positron, antimatter plasmas. One is the development of a method to extract cold beams with small transverse spatial extent from plasmas in a high-field Penning–Malmberg trap. Such beams can be created with energy spreads comparable to the temperature of the parent plasma and with transverse spatial diameters as small as four Debye screening lengths. Using tailored parent plasmas, this technique provides the ability to optimize the properties of the extracted positron beams. In another section, the design of a multicell positron trap is described that offers the possibility to accumulate and store orders of magnitude more positrons than is currently possible (e.g., particle numbers > 10^{12}). The device is scalable to even larger particle capacities. It would, for example, aid greatly in being able to multiplex the output of intense positron sources and in efforts to create and study electron–positron plasmas. This multicell trap (MCT) is likely to also be an important step in the development of portable traps for antimatter. The third topic is a discussion of possible ways to create and study electron–positron plasmas. They have a number of unique properties. These so-called

[a] This chapter, with corrections and minor updates as noted, is reprinted with permission from *Proceedings of the International School of Physics "Enrico Fermi*", "Physics with Many Positrons", Course CLXXIV, in Brusa, R. S., Dupasquier, A., Mills, A. P., Jr. (eds), (IOS, Amsterdam, SIF, Bologna, 2010) pp. 545 – 573.

"pair" plasmas are interesting both from the point of view of fundamental plasma physics and for their relevance in astrophysics.

5.1. Overview

As discussed in the previous chapter,[b] the Penning–Malmberg (PM) trap is the method of choice to accumulate, store and manipulate antimatter plasmas. While that chapter and this one focus specifically upon applications to positron plasmas, the work described here is done with single-component electron plasmas for increased data rate. We are now fully aware how to prepare similar positron plasmas, and the experiments are done in an ultra-high vacuum (UHV) so that annihilation is not a problem. Thus, the extension from the electron to the positron case does not pose any particular difficulties. Chapter 4 described fundamental concepts in the accumulation and manipulation of antimatter plasmas in PM traps. Here we describe three topics that leverage those tools to create important new capabilities in several areas of positron research.

One goal is to develop an efficient way to create cold, bright, pulsed beams of antiparticles. It turns out that confining and cooling the particles in a PM trap allows considerable flexibility and significantly improved capabilities to form such beams. Applications include cold beams for spectroscopy that might be used, for example, to study positron interactions with atoms, molecules and atomic clusters.[2] Another application is the development of new tailored beam sources for materials studies.[3] The techniques described here could conceivably also be useful in producing cold antihydrogen atoms from cold antiproton and positron plasmas. This might, for example, be done by gently pushing a cold, finely focused beam of one species through the other.

A key goal of positron research is to develop methods to accumulate and store the maximum possible number of antiparticles for applications that require "massive" quantities of antimatter and intense bursts of antiparticles. Examples include the creation of electron–positron plasmas[4,5] and the development of portable traps for antimatter. We

[b] Table 4.1 in the previous chapter lists the standard parameters that describe these plasmas in the notation that will be used here.

describe here a scheme to do this, namely a "multicell trap" consisting of a suitable arrangement of PM traps contained in a common magnetic field and vacuum system.

Finally, we discuss possible scenarios to create and study electron–positron plasmas (so-called "pair plasmas"). Due to their characteristics, namely equal-mass particles with opposite signs of charge, they have a number of unique properties. In particular, nonlinear processes proceed very differently in these plasmas as compared to conventional plasmas in which the ion electron-mass ratio is three orders of magnitude larger. Relativistic pair plasmas are of particular interest in astrophysics. For example, copious amounts of this material are believed to be present in the magnetospheres of pulsars.

More generally, these projects are examples of the many potential contributions that research on the physics of single-component plasmas can make to the advancement of science and technology with antimatter.

5.2. Extraction of Beams with Small Transverse Spatial Extent

Specially tailored particle beams have found a myriad of applications in science and technology. This is especially true in studies involving antimatter.[5] Numerous examples involving antimatter are discussed in this volume and at the workshop upon which it is based. For many applications, it is desirable to have beams with a small energy spread and small transverse spatial extent. For a single-component plasma in a PM trap, the space-charge potential is largest on the axis of the plasma. Recently, we exploited this fact to create beams of small transverse spatial extent. This was accomplished by carefully lowering, in a pulsed manner, one of the confining end-gate potentials. This work is described in more detail in references[6–8]. The discussion presented here relies very heavily on that work. Here we describe the main results; glossing over the mathematical details. The experiments to test the predictions of the theory were done with electron plasmas for increased data rate.

A schematic diagram of the experimental arrangement and the electrostatic potential profile in the PM trap for pulsed extraction is shown in Figure 5.1. One quantity of interest is the radial profile of the

extracted beam. Also of interest are the minimum possible beam diameter and the maximum number of particles that can be extracted in a pulse at this diameter.

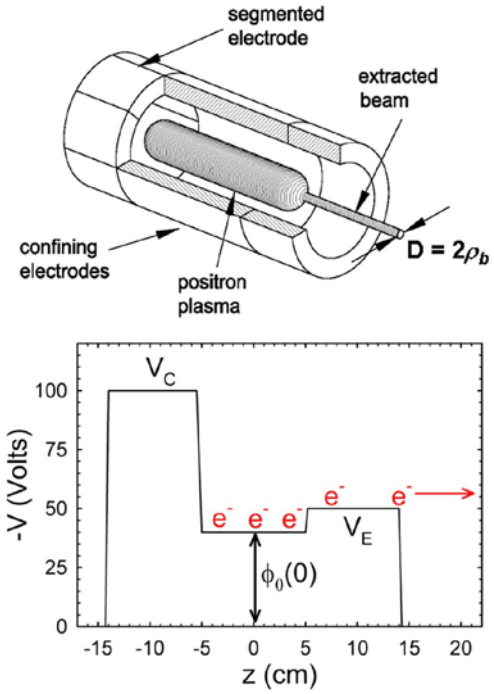

Fig. 5.1. (above) A cartoon of the experimental arrangement used to extract beams of small spatial extent from a single-component plasma in a PM trap; (below) potential profile in the vicinity of the trapped plasma (in this case electrons) in the direction along the confining magnetic field. A focus of the research described here is determining the minimum beam radius, ρ_b, and the other characteristics of the beam pulses.

The Penning–Malmberg trap used for these experiments is in a 4.8 T magnetic field. The corresponding cyclotron cooling time is $\tau_c = 0.16$ s. The trap electrodes had an inner diameter of 2.54 cm. The plasmas are typically in equilibrium, and thus they have a constant density n_0 (i.e., a flat-top radial distribution). They undergo an E x B rotation at the frequency f_E set by n_0. The plasma temperature T is set by the balance between heating sources due to background drag and/or rotating-wall

(RW) torques and the cyclotron cooling. Typical plasmas had a total number, N_0 = 4 x 10^8 electrons, a density n_0 = 1 x 10^9 cm^{-3}, plasma radius, r_p=0.1 cm, plasma length L_p =15 cm and T=0.05 eV (i.e., ~ twice the ambient temperature of 300 K). For these plasmas, the Coulomb collision time, τ_{ee} = 1 ms,[9,10c] is rapid compared to the cooling time, τ_c, thus ensuring that the plasmas are in a thermal equilibrium state.[11]

The plasma potential is largest at the (radial) center of the plasma and constant in the direction along the magnetic field due to plasma shielding (i.e., until one enters the small, "sheath" region at each end of the plasma). To extract a narrow beam, the confining potential, V_C, at one end of the plasma is carefully lowered to a predetermined value by applying a 10 μs square-wave pulse with amplitude ΔV. This extraction time is set by the fact that, as shown in Figure 5.2, the particles escape in a time ~ 5 μs.[7] Shown in Figure 5.3 is an example of the areal (two-dimensional) plasma density of the beam pulse as measured on a phosphor screen, together with charge-coupled device (CCD) images of the trapped plasma before and after beam extraction. As discussed below, the beam width depends upon the end-gate potential, V_E. Smaller-amplitude beams are narrower in diameter. Note that the beam extraction leaves a small "hole" (i.e., a region of decreased plasma density) at the center of the plasma. This hole moves coherently to the plasma edge and disappears in times ≤ 500 μs.[7]

---

[c] There are many considerations when calculating collision rates in cold, magnetized plasmas. These rates depend upon the plasma density n, the cyclotron radius r_c, the Debye length λ_D and the "distance of closest approach" $b \equiv e^2/(4\pi\varepsilon_0 T)$, where T is the plasma temperature. For the plasmas considered here, typically $b << r_c << \lambda_D$, in which case the rate of approach to thermal equilibrium is $\nu_{ee} = Cnb^2 v_T \ln(r_c/b)$, where v_T is the thermal velocity of the particles, and C is a constant of order of unity. The details and other interesting regimes are discussed in reference[10].

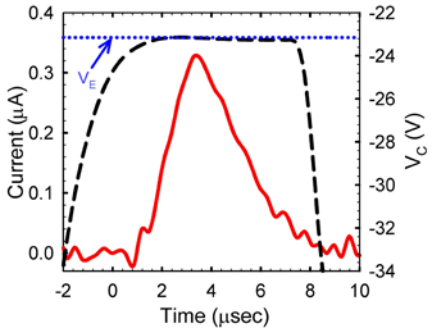

Fig. 5.2. (solid curve) Beam current as measured on a collector as a function of time in response to an approximately 10 μs reduction of the confining potential, V_C, (dashed curve) on one end of the plasma. Data from reference[7]; see this reference for details.

A simple theory was developed to describe the beam extraction process.[7,8] *A key assumption is that the particles do not scatter during beam extraction and that the fastest particles leave first*, with slower particles leaving sequentially depending upon their energies. While plausible, this is not strictly correct and should be checked experimentally, particularly in the case of cold, dense plasmas. Nevertheless, with this assumption, the energy and spatial distribution of the beam pulse can be calculated by simple integrals over the particle distribution in the plasma. Further, as shown below, these predictions are in good agreement with the results of experiments over a relatively wide range of plasma parameters.

The key piece of physics determining the properties of the extracted beam is that the exiting beam particles reduce the plasma potential in the extraction region, and this tends to inhibit more particles from leaving. The point is that the large value of the space-charge potential at the plasma center "pushes" the particles out of the trap. As particles are extracted, this potential decreases most at the radial center of the plasma, the radial potential profile is thus flattened near the plasma center and particles are then extracted over a region of larger radial extent. Since this perturbation in the potential depends upon radius, it can produce non-trivial radial beam profiles.

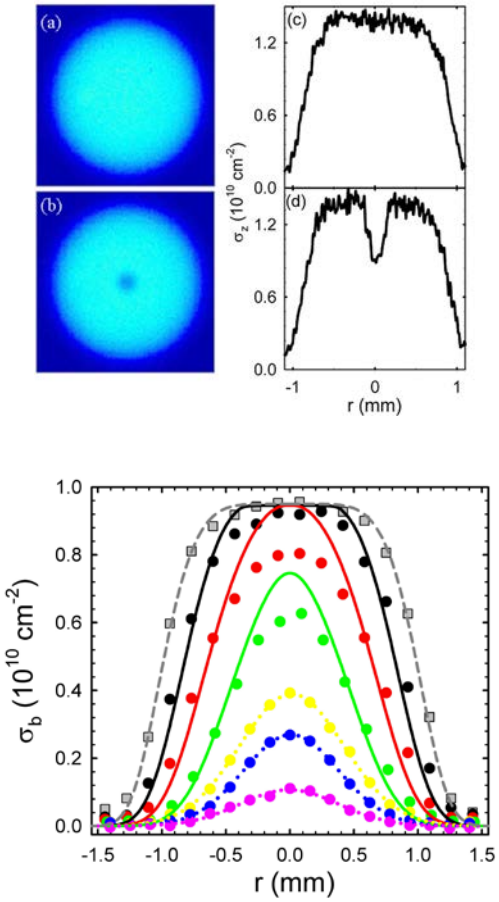

Fig. 5.3. (above) CCD camera images of the (two-dimensional) areal density profiles (a) before; and (b) 10 μs after beam extraction; shown in (c) and (d) are the corresponding radial profiles, $\sigma_z(r)$; (below) profiles, $\sigma_b(r)$, of extracted beams are shown for a selection of normalized beam amplitudes ξ, defined in Eq. (5.3) below: $\xi \approx 0.1, 0.3, 0.5, 1.0, 1.9, 2.8$. Shown for the three smallest beams are Gaussian fits (···), while the three largest beams are fit (–) to numerical solutions. The initial plasma profile, $\sigma_z(r)$, is also shown (■). Negative and positive values of r denote data along a chord through the plasma. Reprinted from reference[7].

As described in reference[7], assuming extraction from a long, cylindrical plasma, the areal density profile of the beam at a given radius

can be written as a simple integral over the particle distribution function, with the lower limiting velocity in the integral $v_{\min}$ set by the extraction voltage, V_E. Thus

$$\sigma_b(r) = 2L_p \int_{v_{\min}}^{\infty} f(r, v_{par}) dv_{par}, \tag{5.1}$$

where v_{par} is the velocity of the particles in the direction of the magnetic field, and

$$v_{\min}(r) = \left[\frac{-2e}{m} \left(V_E - \phi_0(r) + \Delta\phi(r) \right) \right]^{1/2}, \tag{5.2}$$

where $-\phi_0(r)$ is the potential profile before beam extraction (i.e., the explicit minus sign is for the electron plasmas studied here), and $\Delta\phi(r)$ is the change in the plasma potential due to the extraction of the entire beam pulse.

For small-amplitude beam pulses, a simple analytic expression can be derived from Eq. (5.1) to describe the radial beam profile, taking $\phi_0(r)$ and $\Delta\phi(r)$ as that calculated for "flat-top" (i.e., constant-density) radial distributions for the background plasma and the extracted beam, respectively. The areal density profile of the beam is a Gaussian radial distribution,

$$\sigma_b(r) = \sigma_{bo} \exp\left[-\left(\frac{r}{\rho_b} \right)^2 \right]. \tag{5.3}$$

For the smallest-amplitude beams, where $\Delta\phi$ can be neglected, the characteristic radius, $\rho_b = 2\lambda_D$ [HW to 1/e], where λ_D is the Debye screening length. Qualitatively, λ_D is the smallest distance over which a change can be made in the plasma potential, and thus it sets the minimum transverse size of the beam. Since $\lambda_D \propto (n/T)^{1/2}$, extraction from a colder, higher-density plasma will produce narrow beams.

For larger beams, the expression for the width is found to depend upon the change in space charge due to the extracted beam. The critical parameter determining "small" and "large" beams is,[7]

$$\xi \equiv \frac{N_b}{N_0}\left(\frac{rp}{2\lambda_D}\right)^2 = \frac{e\Delta\phi}{T}, \tag{5.4}$$

where N_b/N_0 is the fraction of the *total* plasma particles, N_0, extracted in the beam pulse, r_p is the plasma radius, and $\Delta\phi$ is the difference in space-charge potential across the beam. In terms of this parameter, and taking $\phi_0(r)$ and $\Delta\phi(r)$ as above,[d] the beam radius for Gaussian beams is found to be[7],

$$\rho_b = 2\lambda_D\left[1+\xi\right]^{1/2}. \tag{5.5}$$

When $\xi \geq 1$, the beam profiles depart significantly from the predicted Gaussian profiles. In this case, the profiles can be calculated numerically (i.e., again using the assumption that particles exit the plasma before scattering or radial diffusion occurs). As shown in Figure 5.3, the profiles of small-amplitude beams fit well with the Gaussian predictions, and the profiles of larger-amplitude beams are in reasonable agreement with the numerical calculations. As shown in Figure 5.4, the predicted *beam widths* from Eq. (5.5) are in good agreement with the data over the wide range of the beam amplitudes studied. In fact, the agreement for $\xi > 1$ cannot be justified by the theory and thus appears to be fortuitous.

Key results of this analysis are that the beam radius is limited to $\rho_b \geq 2\lambda_D$ and that this limiting value of $2\lambda_D$ can be readily achieved. Another important result is the identification of ξ as the parameter determining the beam widths. Equations (5.4) and (5.5) set a limit on the fraction of beam particles that can be extracted at the minimum diameter of $4\lambda_D$, namely that $N_b/N_0 << (2\lambda_D/r_p)^2$. Physically, this is the condition that the areal density within the pulse is small compared to the areal density of

[d] Assuming a flat-top, radial beam distribution *in lieu* of a Gaussian distribution makes a negligible error in the calculation of $\Delta\phi$ and ρ_b.

the parent plasma. Equations (5.4) and (5.5) also quantify the beam widths for larger beam pulses.

In practical applications, one would like to convert as much of a trapped plasma into a train of approximately identical pulses as possible. Shown in Figure 5.5 is an example where over 50% of the plasma was converted to a train of 20 nearly identical pulses. It is important to note that this was accomplished by maintaining the central plasma density constant throughout the extraction process using RW compression (cf., the previous chapter, Chapter 4) to keep the plasma density, and hence λ_D constant. After extraction of the beam pulses, the "holes" left by the extracted pulses propagate coherently to the plasma edge in a time < 1 ms. This returns the plasma to a rigid rotor, thermal equilibrium state. This would, in principle, allow pulse extractions at a kilohertz rate. Whether this is possible, given the fact that the plasma must be compressed with the RW to maintain constant *n and* λ_D, is an important topic for future research.

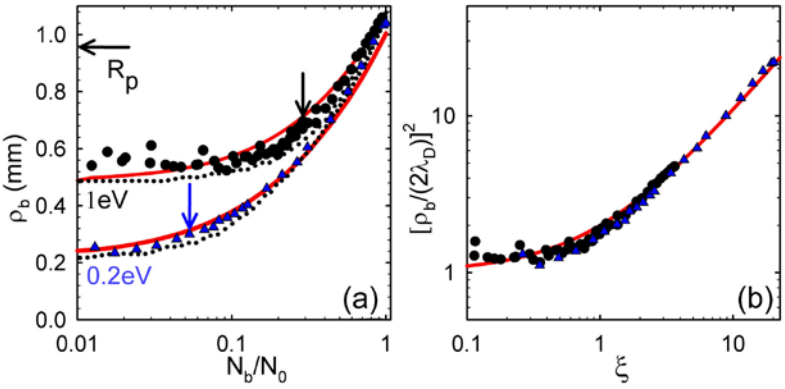

Fig. 5.4. (a) Beam-width, ρ_b, plotted vs. N_b/N_0 for T = 1.0 eV (●), and 0.2 eV (▲). The predictions (–) from Eqs (5.1) and (5.2) are also plotted, with no fitted parameters; (···) shows a numerical calculation from Ref.[7]; arrows correspond to beams with $\xi = 1$. (b) Data from (a) plotted as $(\rho_b/2\lambda_D)^2$ vs the dimensionless beam amplitude ξ, demonstrating the scaling predicted by Eq. (5.5). Reprinted from reference[7].

The energy distribution in the extracted beam is also of importance in many applications, such as when one wants to bunch the particles in time in positron-atomic physics (spectroscopic) applications or to study the energy dependence of certain processes such as vibrational or electronic excitation by positron impact. Recently, a detailed investigation was conducted of the energy distributions of the beam pulses formed in the manner described above.[8]

It is useful to define the dimensionless exit-gate voltage,[8]

$$\eta = (e/T)\left[V_E - \phi_0(0)\right]. \tag{5.6}$$

In terms of η, the beam amplitude can then be written,[8]

$$\xi = (1+\xi)\left[\frac{A\left(e^{-A^2}\right)}{\sqrt{\pi}} - \left(A^2 - 0.5\right) erfc(A)\right], \tag{5.7}$$

where

$$A = \left[\eta + \xi\left(\gamma + 2\ln\left(\frac{R_w}{\lambda_D}\right) + \Gamma\left(0, \frac{R_W^2}{\rho_b^{\,2}}\right)\right)\right]. \tag{5.8}$$

Here, R_w is the inner radius of the electrodes, and Γ is the upper, incomplete gamma function. Using the variables η and ξ, the distribution in energies $E_{||}$ of the beam particles in motion parallel to the magnetic field, can then be written

$$= \frac{1}{e}\frac{dN_b}{dE} = \frac{e^2}{L_p}\frac{d\xi}{d\eta}. \tag{5.9}$$

Thus, by measuring N_b as a function of the extraction voltage V_E (i.e., η in scaled variables), one can measure the parallel energy distribution of the beam. Typical data for N_b[8] are shown in Figure 5.6.

The beam parallel energy distributions, shown in Figure 5.7, are then obtained using Eq. (5.9).[12] Note that for a small number of extracted particles, $\xi = 0.02$, the distribution is fit well by the tail of a Maxwellian, whereas for $\xi = 0.4$, there is a distinct departure from this limit (i.e., due to the change in the plasma potential due to the extraction of the pulse). The dispersion in the total energy of the beam is defined by

$$\Delta E = \left(\left\langle E^2 \right\rangle - \left\langle E \right\rangle^2 \right)^{1/2}. \tag{5.10}$$

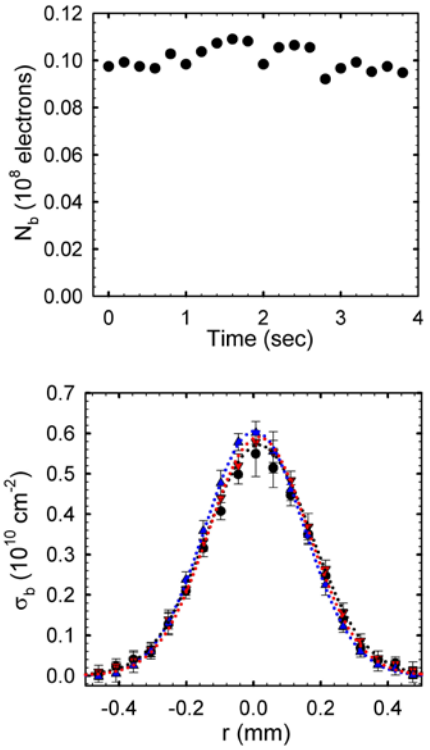

Fig. 5.5. (above) Amplitudes, N_b, for 20 pulses extracted consecutively with $\langle N_b \rangle = 1.0 \pm 0.05 \times 10^7$ and $\xi \approx 0.2$; (below) corresponding areal density profiles for the 1st (●), 10th (▲) and 20th (▼) extracted beams. The pulse amplitude and the radial beam profile remain constant, due to the fact that the density, and hence λ_D, is maintained constant by RW compression during the extractions; Gaussian fits to the profiles are also shown. Reprinted from reference[7].

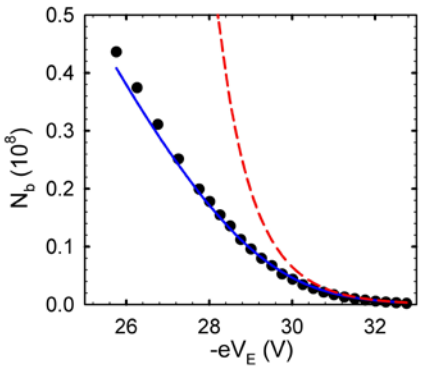

Fig. 5.6. (●) The number of beam particles, N_b, as a function of the extraction voltage, V_E; (solid line) the predictions of the theory of Eqs (5.7) – (5.9); and (——) the result using the small-beam approximation, $\xi \leq 1$. Reprinted from reference[8].

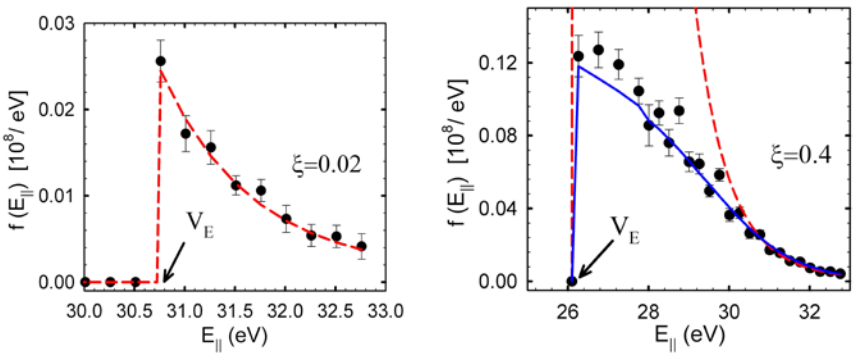

Fig. 5.7. Parallel energy distributions for two values of ξ: (——) prediction of the small–beam approximation; and (–) solutions of Eqs (5.7)–(5.9), compared with (●) the distribution obtained by taking the derivative of N_b as a function of V_E (i.e., dξ/dη). Reprinted from reference[8].

Using Eqs (5.7)–(5.9), the parallel energy distribution function, $f(E_{||})$, and hence ΔE, can be calculated over a wide range of plasma parameters. Here it is assumed that the particle energy distribution in the motion in the plane perpendicular to B is a Maxwellian at temperature T.

As shown in Figure 5.8, the root mean square (rms) energy spread of the extracted beam, increases only modestly with increasing ξ.

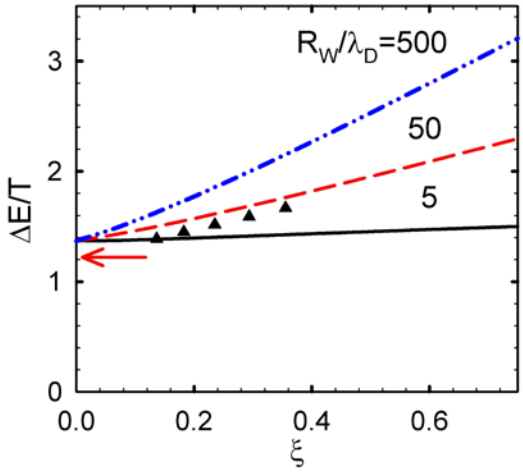

Fig. 5.8. Predictions for the rms spread in the total energy of the beam as a function of ξ for three values of R_W/λ_D (lines), compared with data (▲) for R_W/λ_D = 50. From reference[8]; see this reference for details.

There are a number of potential applications of the beam extraction technique described here. One example is in positron-atomic physics studies, where a magnetically guided beam (i.e., most compatible with extraction from parent plasmas in a PM trap) has distinct advantages.[2] However, there are also situations in which an *electrostatic,* as opposed to a magnetically guided, beam is desirable (i.e., a beam in a B-field free region). In particular, the electrostatic beams admit to the use of electrostatic focusing and remoderation for brightness enhancement.

In reference[7], an example is given of what could be done extracting a cold beam ($T \sim 10$ meV) from a cryogenically cooled plasma in a 5-tesla field. Assuming it is guided to a region where $B \sim 5$ gauss (5×10^{-4} T) and then extracted from the field, an electrostatic beam could be formed with a diameter of 1 mm and an energy spread of 10 meV (essentially all of which is in the perpendicular direction). Such a beam would be a considerable advance for positron-atomic physics scattering experiments and for certain types of materials analysis. For example, typical electrostatic beams used for atomic physics studies have energy spreads

≥ 0.5 eV and transverse extents ≥ 5 mm. There is a limit, however, on N_b for these cold, small-diameter beam pulses. To keep $\xi < 1$ and form a beam with an energy spread of 10 meV, for example, the number of particles per pulse is $N_b = 4 \times 10^3$.

In 2010, Weber and collaborators developed a method to extract particles tailored in a high-field PM trap (i.e., as described here) from the magnetic field to create a new class of electrostatic beams[13]. We refer the reader to reference[13] for details. Such beams are useful in a range of applications, including positron scattering studies involving atoms and molecules.[2] They are also important in that other methods to brightness-enhance beams such as "remoderation"[14] can be used once the particles are in a magnetic-field-free region.

5.3. Multicell Trap for Storage of Large Numbers of Positrons

Overview. Many applications require large numbers of positrons and/or long storage times. Furthermore, great benefits are anticipated if one could develop a *portable* antimatter trap. This would permit decoupling the end use of the antimatter from the source of the antiparticles, be it a particle accelerator, a nuclear reactor or even a compact, sealed radioisotope source. They are all awkward to deal with in many applications. While portable antimatter traps have been discussed previously,[5,15,16] none have yet been developed.

We describe here the next key step in research to develop a next–generation of positron storage devices. The near-term goal is to increase by orders of magnitude the number of positrons that can be accumulated and stored for long periods. Impediments to further progress include dealing with large plasma potentials. In addition, due to radial plasma transport in the presence of these large space-charge potentials, there are serious barriers to achieving very long confinement times (e.g., days) in these devices.

To achieve these objectives, we describe here the design of a novel *multicell* Penning–Malmberg trap.[17,18] In this discussion, we refer to a "cell" as a single-component plasma in an individual PM trap, in the case where more than one such plasma is arranged in the same magnetic field

and vacuum chamber. The basic idea is that this MCT can confine and store antiparticles in separate plasma cells, shielded from one another by copper electrodes. These electrodes screen out the plasma space-charge potential, in turn reducing the required confinement voltages for a given number of particles by an order of magnitude or more. Such MCTs have been developed previously for other applications, namely arrays of quadrupole mass spectrometers used to increase sample analysis throughput.[19,20]

The initial goal is to develop a device in a common magnetic field and vacuum system that can store $\geq 10^{12}$ positrons for days or weeks without significant losses. As illustrated in Figure 5.9, this would increase the present state of the art by a factor $\sim 10^2 - 10^3$. Such a device would also represent a major step toward the development of a versatile, portable antimatter trap.

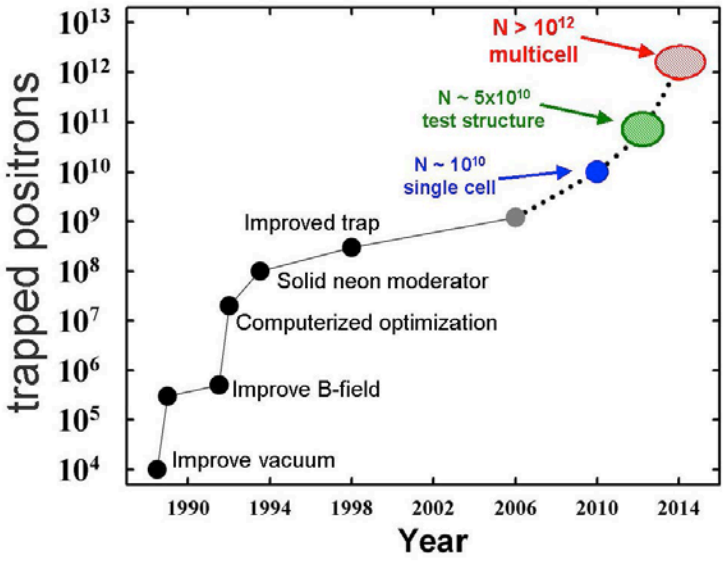

Fig. 5.9. Progress in positron trapping from similar strength sources of ~ 50 – 100 mCi ^{22}Na using a buffer-gas accumulator, including stacking positron plasmas in UHV;[5,21–23] (oval, UCSD) parameters achieved for an electron plasma, and (oval, multicell) the expected value for the MCT described here (updated in 2012).

The concept of the multicell PM trap is shown schematically in Figure 5.10.[17] There are several potential factors limiting long-term confinement of large numbers of positrons in PM traps. One is the Brillouin limit (cf., Section 4.4), which is the limiting density for plasma confinement in a uniform magnetic field. For electrons or positrons at tesla-strength magnetic fields, the Brillouin limit is beyond the capability of present-day experimental capabilities, and so (albeit unfortunately) it is not of immediate concern. A more important near-term limitation is the effect of plasma space charge, which is a key practical constraint for present-day positron traps. For large particle numbers, N, the space-charge potential of a cylindrical, single-component plasma of length L_p in a PM trap is proportional to N/ L_p. For a fixed plasma length L_p, the number of particles, N, that can be stored in a trap is limited by the maximum potential, V_C that can be applied to electrodes in vacuum, in the presence of the plasma.

As described in Chapter 4, typical cylindrical plasmas in PM traps are space-charge limited at ~ $10^{11}\,\tilde{V}_C$ particles per meter of plasma length, where $\tilde{V}_C$ is the confining potential in kV (cf. Chapter 4).[17] For example, for a plasma of 10^{10} positrons with L_p = 0.1 m and r_w/r_p = 8.8, the plasma potential is 750 V, which, in turn, requires a value of V_C > 750 V. While this value of V_C can be achieved relatively easily, the maximum possible operating potential for a compact PM trap, with closely spaced electrodes used to confine large numbers of electron-mass particles in a strong magnetic field, depends upon the specifics of the apparatus and must be demonstrated experimentally.

Another consideration arises from the fact that the heating due to outward diffusion is proportional to the plasma potential (cf. Chapter 4 and reference[17]). This heating can inhibit the ability to confine and compress positron plasmas. It can also lead to positronium (Ps) formation on background impurities in the vacuum system, and this represents a potentially serious positron loss process. For typical vacuum system contaminants, Ps formation has an energy threshold of several electron-volts and a relatively large cross-section ~ 10^{-20} m^2. The resulting neutral Ps atoms will annihilate quickly. To avoid this loss, the

positron plasma must be kept relatively cool (e.g., $T \leq 2$ eV), and so unnecessary plasma heating must be avoided.

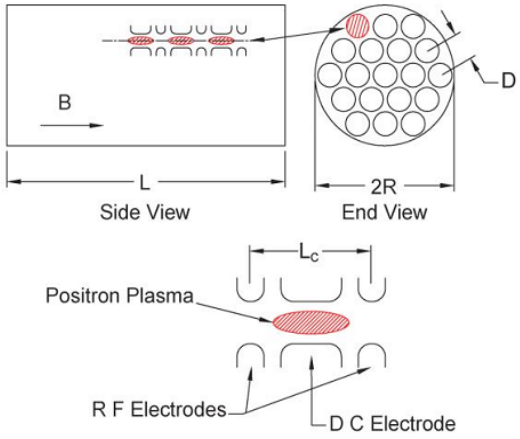

Fig. 5.10. Conceptual design of an MCT, showing the arrangement of cells parallel and perpendicular to the several-tesla magnetic field, B. This device consists of hexagonally close-packed cells perpendicular to the magnetic field and a number of in-line cells in the field direction. RF = radio frequency; DC = direct current.

As shown in Figure 5.10, a key feature of the MCT is that large values of the plasma potential (i.e., due to the space charge of the plasma) can be mitigated by dividing the plasma into m, rod-shaped plasmas. Each plasma, of length L_p, is oriented along the magnetic field in a hexagonal-close-packed (HCP) arrangement transverse to the field. These rod-shaped plasmas are shielded from each other by closely fitting copper electrodes. For a given maximum confining electrical potential V_C, the number of stored positrons will be increased by a factor of m. Since the plasma heating rate due to outward expansion of the plasma is proportional to the potential drop across the plasma, the multicell design also reduces the requirements on plasma cooling. In the trap design considered here, cooling is accomplished by cyclotron radiation of the particles in a relatively large (e.g., several-tesla) magnetic field.

The multicell design also breaks up each long rod of plasma into p separate plasmas in the direction along the magnetic field (i.e., separated by electrodes at potential V_c). The plasma length is decreased by a factor L_p/p, and this reduces the effects of magnetic non-uniformities, since many of the cells are now both off the axis of symmetry and away from the mid-plane of the magnet. Breaking up the plasma longitudinally also reduces the rate of outward, asymmetry-driven radial transport (i.e., which is typically found to be proportional to L_p^2 (cf., Chapter 4 and reference[24]). The design parameters for a 21-cell MCT are summarized in Table 5.1. The electrode structure will be cooled to cryogenic temperatures to freeze out contaminant impurity molecules and to ensure a UHV environment. Using rotating electric fields in each cell for radial plasma compression, the positron loss is expected to be small on the design-goal time scale for confinement times of weeks.

Table 5.1. Design parameters of a 21-cell MCT.

Number of cells (m x p = 7 x 3)	21
Total positron number, N (10^{11})	$\geq$ 5.0
Magnetic field (T)	5
Total electrode length, L (cm)	100
Electrode–package diameter, 2R (cm)	> 7.5
Plasma radius, R_P (cm)	0.2
Plasma length, L_p (cm)	20
Confinement voltage, V_c (kV)	1.0
Cell spacing (cm), D	2.0
Space-charge potential (V)	750
Rotating-wall frequency (MHz)	4

The plasma is expected to be considerably warmer than the electrode temperature (i.e., ~ 0.1 eV) due to plasma heating from the radio frequency fields used to achieve long-term plasma confinement. The work reported here used a confinement potential, V_C = 1.0 kV, which resulted in a maximum particle number of N = 3 x 10^{10} in a single PM

cell. The design in Table 5.1 is conservative in this regard. If one could work with ~ 3 kV, which is likely, a trap for 10^{12} positrons would require only 14 cells. Alternatively, a 95-cell trap could confine $\geq 6 \times 10^{12}$ positrons.

To fill the MCT, positrons will be accumulated in a buffer-gas trap using the arrangement shown in Figure 5.11. Typically $N \sim 3 \times 10^8$ e^+ can be accumulated from a 100 mCi ^{22}Na radioactive source and noble gas moderator in a few minutes. The positron plasmas from the buffer-gas trap will be "stacked"[21,25,26] in UHV in the high-field trap[21] with a cycle time of several minute to achieve $\geq 10^{10}$ positrons in a single plasma cell. At these fill rates, trapping 10^{12} positrons would take several days to a week. However, stronger positron sources are currently in operation and/or under development in a number of laboratories around the world that could fill such a trap in a few hours or less.[5,27–29] A master plasma-manipulation cell (on the left side of the MCT) will receive plasmas from the buffer-gas trap, compress them and move them off axis radially by a technique described below, before depositing them in the multiple storage cells.

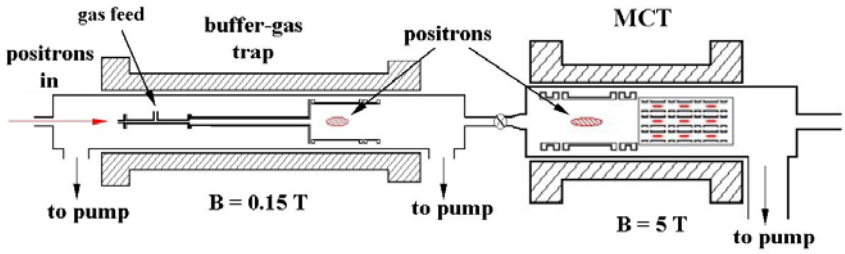

Fig. 5.11. Schematic diagram of the buffer-gas positron trap (left) used to accumulate positrons from a continuous source and shuttle them to the MCT. The buffer-gas trap is connected by a pulsed valve to the high-field UHV, multicell storage trap (right). Positrons from the source and moderator enter the buffer-gas trap from the left. The source could be a conventional radioisotope (^{22}Na) and a solid neon moderator, or a higher intensity source.

Validation of the MCT concept. A series of experiments were performed recently (using test electron plasmas) to validate key procedures necessary to operate an MCT successfully. The experiments

were performed in the cylindrical high-field PM trap described in Chapter 4.[18] Plasmas are confined in various combinations of cylindrical electrodes (r_w = 1.27 cm) to achieve plasma lengths in the range $5 \leq L_p \leq$ 25 cm. The electron plasmas are injected using a standard electron gun and confined radially by an applied 5-tesla magnetic field, with axial confinement provided by voltages applied to the end electrodes. In typical experiments, rotating electric fields (i.e., the RW technique described in Chapter 4) provided long-term confinement. The segmented RW electrodes are also used to excite and detect diocotron modes in the plasma that, as described below, were used to move plasmas across the magnetic field.

The plasmas are cooled by cyclotron radiation in the 5 T magnetic field at a rate, $\Gamma_c \sim 6\ s^{-1}$, [30] which is fast compared to the compression and expansion rates. Steady-state plasmas remain relatively cool (i.e. $T \leq$ 0.2 eV; $T/e\phi_0 << 1$, where ϕ_0 is the plasma potential), even in the presence of strong RW fields. It was established that the steady-state density *could be maintained for more than 24 hours* with no loss of plasma.[18] The dependence of the plasma density on the total number of particles N is illustrated in Figure 5.12 for the three different confinement lengths L_c (i.e., the length of the potential well imposed by voltages on the electrodes) and a 1 kV confinement potential. The ability to create and manipulate two, in-line plasmas was also demonstrated.[18]

One of the key requirements for an MCT is development of a robust and compact method to move plasma across the magnetic field. While this could be accomplished by magnetic deflection or use of ***E x B*** plates, both of these techniques have disadvantages in terms of space requirements and the need to switch large magnetic fields and/or electrical potentials. A method to move plasmas across the field was developed using excitation of a so-called “diocotron mode" of the plasma.[31] Specifically, when a single-component plasma is displaced from the axis of the cylindrical electrode, the center of mass will exhibit an ***E x B*** drift due to the electric field of the image charge of the plasma induced in the electrodes that surround it. This uniform drift of the plasma center at frequency f_D about the axis is called a *diocotron mode*.

The amplitude of this mode is the displacement, D, of the plasma from the axis of symmetry of the confining electrodes.

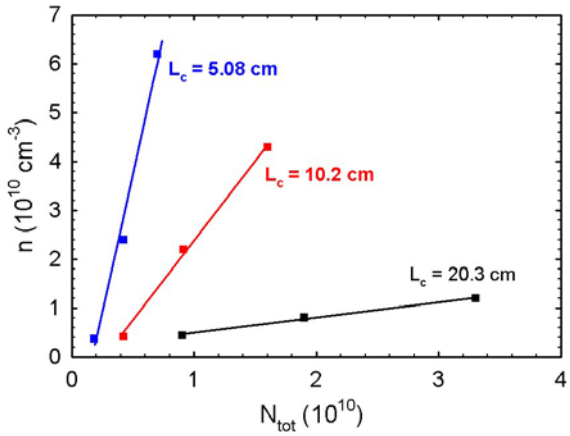

Fig. 5.12. The plasma density, n, as a function of the total number of confined particles, N, is shown for three different confinement lengths, L_c (i.e., the length of the electrodes forming the confinement well), using a confinement voltage, V_C = 1.0 kV. To vary N, three different electron-gun fill voltages were used, 0.3, 0.6 and 0.9 kV, at each value of L_c, represented by the three data points on each line. Reprinted from reference[18].

For a long plasma column with $L_p >> r_w$, the linear frequency of the m_θ=1, $k_z = 0$ diocotron mode is approximately

$$f_D \approx (r_p/r_w)^2 f_E, \tag{5.11}$$

where $f_E = ne(4\pi\varepsilon_0 B)^{-1}$ is the ***E x B*** plasma rotation frequency (cf., Chapter 4 and reference[31]). In these experiments, $f_D \sim$ a few kHz $<< f_E$. The diocotron mode was excited by applying a sinusoidal voltage at a frequency near f_D to one sector of the four-sector electrode. As described below, the technique of "autoresonance" provides an effective and convenient method to control both the amplitude (i.e., radial displacement, D) and the azimuthal position of the plasma column as a function of time.

As the diocotron mode grows in amplitude and the plasma moves further off axis, the mode frequency changes. To lowest order, assuming $r_p << r_w$, the nonlinear diocotron frequency f_{NL}[32] is

$$f_{NL} = f_D \frac{1}{1-\left(D/r_w\right)^2}. \tag{5.12}$$

Figure 5.13 shows a comparison of the measured values of f_{NL}/f_D as a function of D compared to the predictions of Eq. (5.12).

In the experiments, plasmas could be imaged directly with CCD camera out to a displacement D ≈ 0.45 cm (r_w = 1.27 cm). Beyond that radius, D was measured using a pick-up signal on a segmented electrode.[18] A plasma displacement corresponding to 80% of the electrode radius was achieved. This has important, positive, implications concerning the ability to completely fill an electrode structure with multicell plasmas by addressing cells far from the magnetic axis.

The plasma could be phase-locked to a drive signal using the technique of "autoresonance". Autoresonance is the tendency of a driven nonlinear oscillator to stay in resonance with the drive signal, even when the system parameters are varied. This phenomenon was explored in some detail by Fajans *et al*.[33–35] for the case we are interested in, namely the diocotron mode. Using this technique, the diocotron mode is brought into autoresonance by sweeping the drive frequency from below the linear diocotron frequency to a selected, higher frequency. If the drive voltage is sufficiently strong, the excited diocotron mode amplitude (i.e., the displacement, D, of the plasma column from the symmetry axis) will grow as the mode increases in frequency with the drive frequency. In the autoresonant condition, the excited diocotron mode stays phase-locked to the applied signal. We plan to use this technique to inject trapped plasmas into the off-axis cells in the MCT, and we conducted experiments with electron plasmas to test this.

Figure 5.14 shows a model calculation to illustrate the autoresonant response of a plasma of relatively small spatial extent to a constant-amplitude sine wave, $V_D = V_o \sin(2\pi ft)$, as the drive frequency, f, is

changed. The initial on-axis plasma is driven to a large displacement when the frequency of the drive is swept from below the linear mode frequency to a higher frequency. The final displacement, D, is determined by the final frequency of the applied signal. The angular position of the plasma in the plane perpendicular to the B-field is determined by the phase of this applied signal.

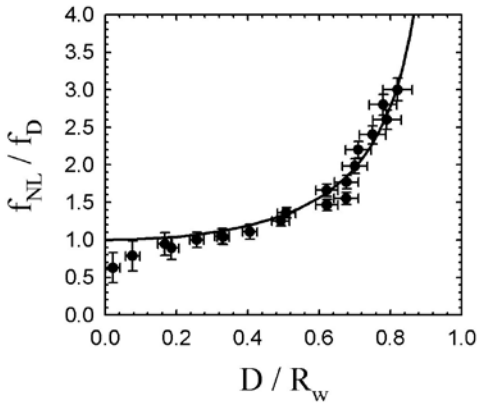

Fig. 5.13. The diocotron frequency (●) measured for plasmas displaced different distances D from the electrode center; and (—) the prediction of Eq. (5.12) with no fitted parameters. The linear diocotron frequency is f_D = 2.9 kHz. From reference[18].

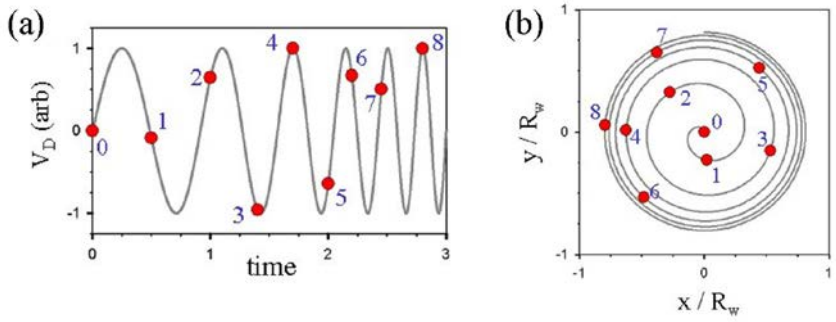

Fig. 5.14. Model calculation of the evolution of the plasma position during the excitation of a nonlinear diocotron mode in the condition of autoresonance: (a) the drive voltage $V_D(t)$ as a function of time in units of the period, τ_1, of the linear diocotron mode; and (b) the corresponding plasma orbit in the (x, y) plane perpendicular to the magnetic field at various times. Numbers correlate the plasma position with the phase of the drive signal. As the frequency increases, the plasma column moves to larger displacements.

Figure 5.15 (left panel) shows CCD images of autoresonantly excited plasmas that have been deposited on the screen at a fixed phase angle, $\phi = 0^{o}$, in the plane perpendicular to B. Note that these displacements are much larger than the plasma radius, demonstrating that $D >> R_p$ can be achieved. The ability of this technique to deposit plasmas at four predetermined *azimuthal* locations (90° apart) is shown in the right-hand panel of Figure 5.15. These experiments demonstrate that the autoresonance technique will enable depositing plasmas in cells at arbitrary locations in the plane perpendicular to the magnetic field. These results indicate that plasmas can be moved across the magnetic field in a few milliseconds or less and can be deposited in specific off-axis cells to a high degree of accuracy (e.g., +/– 0.2 mm in the radial and azimuthal directions).

The process of filling the MCT is illustrated schematically in Figure 5.16. Plasmas from a buffer-gas positron accumulator will be shuttled into a master plasma manipulation cell (left), then the dicotron mode will be excited to the appropriate values of displacement D and phase angle ϕ before the plasma is deposited into a specific off-axis cell. Shown in Figure 5.17 is a schematic illustration of the design of an electrode structure for a 21-cell trap (i.e., compatible with the design parameters summarized in Table I). It incorporates a master plasma manipulation cell for injection into off-axis cells. Each storage cell has a segmented electrode for RW radial plasma compression, an equal-length dc electrode, and confinement electrodes at each end.

Using the RW technique in the strong-drive regime (cf. Chapter 4), plasmas with a remarkably broad range of initial densities (e.g., varying by a factor of 20 or more) can be compressed to a given final-state density by the application of a single, fixed RW frequency. This results in considerable simplifications in the design of a practical MCT. In particular, in this regime of RW operation, active control and interrogation of individual plasma cells is unnecessary. This strong-drive regime also has important consequences in reducing plasma heating. As discussed in Chapter 4, this is due to the fact that the mismatch in frequencies between the plasma rotation and the RW drive is negligibly

small, and this minimizes the RW heating. Thus, operation in the strong-drive regime approximates closely the minimum possible heating rate.

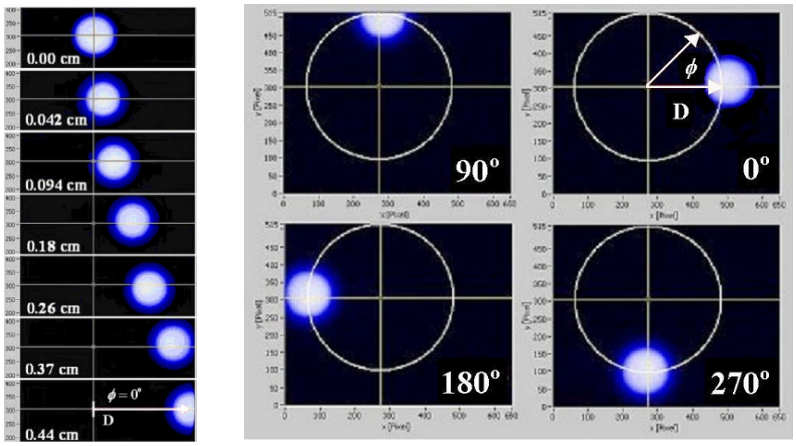

Fig. 5.15. CCD images of plasmas displaced from the axis by autoresonant excitation of the diocotron mode and dumped onto a phosphor screen: (left) six radial displacements at fixed azimuthal position; and (right) four azimuthal displacements at a fixed radial position. From reference[18].

The experiments indicate that it will be possible to access plasma parameters of $n \geq 5 \times 10^{15}$ m^{-3} at B = 5 T. In this regime, the outward transport rate, Γ_o, is independent of plasma density (i.e., instead of increasing as $\Gamma_o \propto n^2$ which is the case at lower plasma densities[11,36]). This too reduces the required RW drive torque and thus leads to considerably less plasma heating, and so the plasmas remain cool. Plasmas with parameters such as those listed in Table 5.1 can be created with T~ 0.1 eV. This is ideal for the multicell positron trap. As discussed above, one important consideration is keeping the plasma temperature sufficiently low so that one can avoid Ps formation by collisions of positrons with background gas molecules. The relatively low values of plasma temperature reported here, namely $T \leq 0.5$ eV, easily fulfill this requirement.

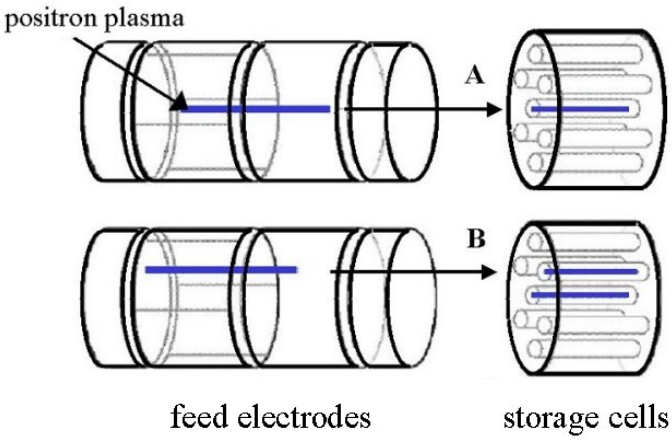

Fig. 5.16. Injection of plasmas into specific cells in the MCT: phase-dumped into an (A) on-axis, and (B) off-axis plasma cell.

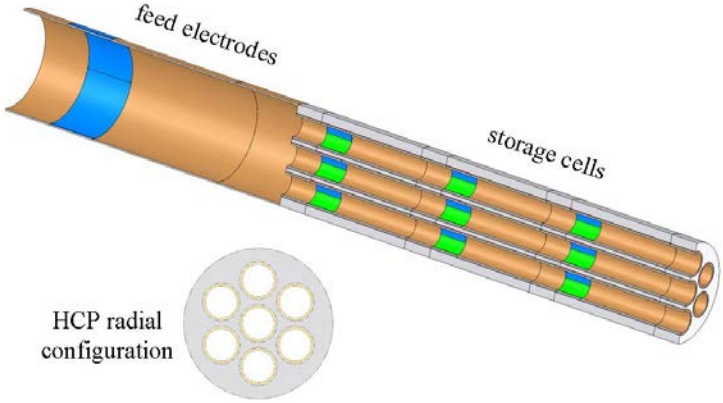

Fig. 5.17. Schematic diagram of the 21-cell multicell positron trap, showing three banks of seven cells in an hexagonally closed packed arrangement. Plasmas from the source will first enter the feed electrodes, then be moved off axis using autoresonant excitation of the diocotron mode to fill off-axis storage cells.

Summary. Key techniques have been demonstrated that will be critical to the development of a practical multicell positron trap. Specifically, operation of the trap at confinement potentials of 1 kV has been demonstrated, resulting in the ability to store $\geq 10^{10}$ particles (in this case electrons) in a single cell. The ability to operate two plasma cells simultaneously was established. Finally, to fill off-axis cells, diocotron-mode excitation of plasmas to a displacement 80% of the electrode radius and phased dumping these plasmas were demonstrated with a precision that exceeds that required for a practical positron trap. These results validate key aspects of the design of the multicell positron trap for $N \geq 10^{12}$ positrons. Further multiplexing can potentially increase the trap capacity by additional orders of magnitude beyond this benchmark goal.

In 2012, the University of California, San Diego (UCSD) Positron Group began to build a 21-cell MCT for 10^{12} positrons along the lines of that described in Table 5.1 and shown schematically in Figure 5.17.

5.4. Electron–Positron Plasmas

Electron–positron plasmas ("pair plasmas") are exceedingly interesting physical systems for a number of reasons. While there have been extensive theoretical studies of electron-positron plasmas,[37–43] there have been few attempts to study them experimentally. The major problem in conducting such experiments is that they are neutral plasmas (or approximately so). Thus the powerful confinement theorem for single-component plasmas (cf., Chapter 4) is inapplicable. Thus achievable confinement times for pair plasmas are expected to be many orders of magnitude shorter than those for pure positron plasmas, and this poses a huge challenge to experimentalists. However, with the advent of high-intensity positron sources and means to accumulate large numbers of positrons (e.g., the MCT described above), we are on the verge of creating these interesting plasmas in the laboratory.[e] Much of the

[e] For the (tenuous) pair plasmas considered here, Ps formation and positron annihilation with electrons can be neglected. The annihilation time for a positron in an electron plasma with density $\sim 10^{20}$ m^3 is approximately 1 s, independent of the plasma temperature. The rates of other processes, such as $e^+ + e^- \rightarrow Ps + h\nu$ and $e^+ + e^- + e^- \rightarrow Ps + e^-$, are also expected to be small.

following discussion follows closely to that presented in reference[44], albeit with revisions for recent progress. The reader is referred to this reference for further details.

In a seminal paper, Tsytovich and Wharton[45] pointed out that electron–positron plasmas possesses truly unique properties because of the equal-mass, opposite sign-of-charge nature of the plasma particles. For example, cyclotron radiation in these plasmas is linearly, rather than circularly, polarized. Furthermore, the nonlinear behavior of these plasmas is dramatically different than that in conventional electron–ion plasmas. For example, in an equal-mass plasma in which the species are in equilibrium at temperature T, the ion acoustic wave is very heavily damped; three-wave coupling processes (e.g., parametric decay) are absent; and nonlinear Landau damping is larger by the electron/ion mass ratio M/m, as compared to the conventional case. This completely changes the behavior of the plasma.

Relativistic electron–positron plasmas are thought to play a particularly important role in nature. For example, large quantities of this material are believed to be present in the magnetospheres of pulsars. As mentioned above, pair plasmas have been studied extensively theoretically,[39–43] but not experimentally, and thus this topic literally begs for experimental investigation. The first laboratory experiments to study something close to this situation were conducted by passing an electron beam through a positron plasma confined in a Penning trap (i.e., a study of the electron-beam, positron-plasma instability).[46,47] However, it is much more desirable to create an electron–positron plasma in which the two species are not drifting relative to each other.

Various techniques have been proposed for creating such simultaneously confined electron and positron plasmas. They include confinement in a magnetic mirror,[48] in toroidal a magnetic configuration known as a stellarator,[4] and in a combined Penning/Paul trap.[44] Due to the anticipated difficulties in simultaneous confinement of these plasmas, an intense positron source, such as that from a linear electron accelerator (LINAC), or an isotope-producing nuclear reactor such as the Munich fission reactor,[49] is virtually obligatory in order to achieve useful data rates in a laboratory experiment.

As mentioned above, it would be of great interest to study the relativistic regime. A magnetic mirror device is expected to provide good confinement for such a hot, electron-mass plasma. However, at the anticipated high temperatures, the Debye length is comparatively large for a given plasma density. Consequently, relativistic electron–positron plasma experiments will require *very* large numbers of positrons (e.g., $N \geq 10^{15}$ per plasma, with an expected lifetime $\leq$ 1s).[44] This is likely to challenge the capabilities of available positron sources for the foreseeable future.

An alternative approach to study relativistic electron–positron plasmas is the use of intense lasers. While these kinds of experiments are outside the scope of the present review, there has been great progress in this area in recent years, driven by the ever-increasing capabilities of high-intensity laser technology. We refer the reader to references[50–56] for further discussions of this promising new direction. As pointed out in reference[56], one can not only expect to generate very large numbers of positrons with these techniques (e.g., $N \sim 5 \times 10^{11}$), but one could also likely create strong confining magnetic fields using complementary laser-based techniques.

Combined trap for low-density electron–positron plasmas. One method to create and study a low-density, cool electron–positron plasma involves a hybrid trapping scheme.[44] The challenge of simultaneous confinement of both charge species can be overcome by the use of a combination of Penning- and Paul-trap technology. In a Paul trap, one can confine charged particles of both signs of charge by means of radio frequency (RF) fields. The basic concept is that in a rapidly oscillating high-frequency electric field ($\omega >> \omega_p$), the plasma is repelled from regions of large electric field. This concept gives rise to the notion of a ponderomotive force which can be written,[57]

$$\vec{F}_{pon} = -\frac{\omega p^2}{2\omega^2}\vec{\nabla}\left\langle \varepsilon_0 E^2 \right\rangle. \tag{5.13}$$

Regions of large oscillating electric field act as potential hills and thus repel particles of both signs of charge. Paul traps have been used to confine quasi-neutral plasmas of positive and negative ions.[44] More

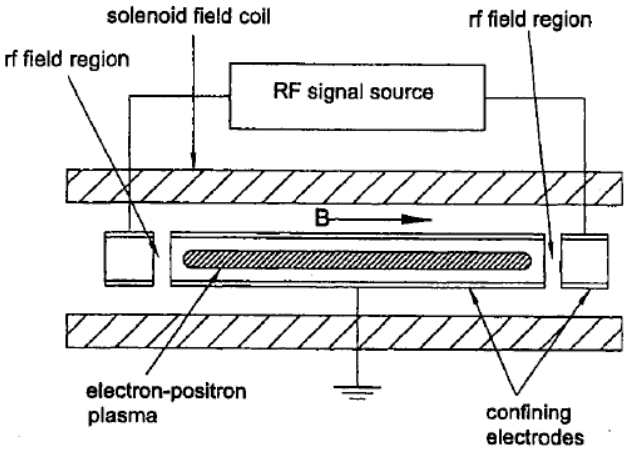

Fig. 5.18. A combined Penning–Paul trap for studying electron–positron plasmas. A uniform magnetic field B will provide confinement for both signs of charge in the direction perpendicular to B. RF fields at each end provide confinement in the direction along B. These large, high-frequency electric fields peak near the location at which the end and central electrodes meet. From reference[44].

recently, the simultaneous confinement of protons and electrons was demonstrated in a trap in which the electrons were confined by RF fields and the protons were confined in an overlapping Penning trap.[58]

In a natural extension of these experiments, we have proposed using a combined trap, illustrated in Figure 5.18, to confine an electron–positron plasma.[17] This would be done using a hybrid, Penning–Paul trap where radial confinement is provided by a magnetic field, as in a Penning trap; and confinement along the magnetic field is provided by RF electric fields E_{rf} (i.e., in place of the electrostatic potentials of the Penning trap). In this design, heating of the species by the RF is a problem. This can be overcome using the cooling provided by small amounts of a suitably chosen molecular gas (as described in Chapter 4).

The design parameters for the experiment are given in Table 5.2. The maximum achievable depth of the potential well using the Paul trapping technique is limited by practical considerations to a few electron-volts,

thereby placing limits on the plasma temperature and the acceptable amount of charge imbalance. For these and other electron–positron plasma experiments, the advantage of using an intense positron source would be that the experiments could be conducted with more rapid cycle times, even if the confinement is relatively poor (which is likely).

Much of the discussion here follows closely that presented in reference[44]. The cooling is due to electron and positron collisions with neutral CO_2 molecules.[f] The steady-state temperature can be estimated by balancing the heating of the particles due to Coulomb collisions in the RF field and the cooling due to inelastic, vibrational, electron–molecule and positron–molecule collisions.[g] The heating rate due to Coulomb collisions will be

$$\frac{d\varepsilon}{dt} \approx 2m\nu_c \left\langle \left(\delta v\right)^2 \right\rangle, \tag{5.14}$$

where ν_c is the Coulomb collision frequency and $\delta v = eE_{rf}/m\omega$ is the particle velocity due to the RF field at frequency ω. It is useful to note

$$\frac{d\varepsilon}{dt} \propto U_{rf} = \frac{e^2 E_{rf}^2}{m\omega^2} \approx m\left\langle \left(\delta v\right)^2 \right\rangle, \tag{5.15}$$

that where U_{rf} is the RF trapping potential energy. The heating rate must be spatially averaged over the trajectory of the particles in the potential well. For a cylindrical plasma of length L, confined by cylindrical electrodes of radius $r_w << L$, with the confining electrode between $z = 0$ and $z = L$, the particles will be heated appreciably only in the regions of large RF electric field. This will occur only near the ends of the plasma in a region of extent $\delta z \sim 0.4\ r_w$ near the turning points of the motion.[44]

---

[f] It is assumed here that the molecular gas is CO_2, but other cooling gases could also be used (e.g., CF_4). It should be noted that SF_6 would not be a good choice because electrons attach to it.

[g] Consistent with the discussion in reference[44], the heating due to charged-particle/neutral, momentum-transfer collisions in the region of the rf fields was neglected. Recent estimates (2012) indicate that this does not significantly change the estimates made here.

To fix the design parameters, a trapping well depth, U_{rf} = 5 eV and a plasma temperature $kT \sim 0.5$ eV are assumed. Near the turning points, the particles experience an RF potential of strength ~ kT/e, and they spend more time near these locations than in other regions of the trap. Taking these factors into account and assuming $L = 30R_w$, the estimate made in reference[44] is that the time-averaged heating rate is,

$$\frac{d\varepsilon_{rf}}{dt} \approx 0.05\nu_c T \quad [h] \tag{5.16}$$

The rate of energy loss will be $d\varepsilon/dt \approx -\nu_{col}\varepsilon_j$, where ε_j is the average energy loss per collision and ν_{col} is the collision frequency for inelastic vibrational excitation of the molecule. We assume that the cooling gas is CO_2, which has a vibrational-quantum energy, ε_j = 0.3 eV, and a collision cross-section $\sigma \sim 10^{-16}$ cm^{-2} (cf., Table 4.1, Chapter 4)[44].[i] With these assumptions

$$\nu_{col} = n_n \sigma v_T \approx 2.0 \times 10^5 P \ \text{[Hz]}, \tag{5.17}$$

where n_n is the CO_2 number density and P is the pressure in millibars. Thus

$$\frac{d\varepsilon_{col}}{dt} = -7.0 \times 10^4 P \ \text{[eV/s]}. \tag{5.18}$$

In steady state, $d\varepsilon_{rf}/dt + d\varepsilon_{col}/dt = 0$. Thus $\nu_c \sim 2 \times 10^6 P$ (Hz). For n = 10^7 cm^{-3} and T = 0.5 eV, $\nu_c \sim 2 \times 10^3$ Hz, which would require a CO_2 pressure of 1.3 x 10^{-6} mbar.

---

[h] The 0.05 factor in Eq. (5.16) accounts for the fact that the heating only occurs in the region of the RF fields. A similar weighting factor would be relevant to electron/positron neutral collisions (cf. footnote below).

[i] Simplifying assumptions were made in that analysis and are continued here. Experiments indicate that for positrons, the cross-section for vibrational excitation is twice the value used here,[2] while the vibrational excitation cross-section for positrons and electrons are taken to be the same. Further, heating due to electron/positron neutral collisions is neglected. Neither is expected to change substantially the estimates made here.

At this pressure, the annihilation time is ~ 80 s, the diffusion time due to collisions with neutral gas is ~ 500 s, the diffusion time due to electron–positron collisions is ~ 200 s, and the Bohm diffusion time[44] is ~ 100 μs. Thus the plasma can be expected to survive between 100 μs and several hundreds of seconds, depending on which transport mechanism dominates. This is an interesting issue in its own right and would likely be one of the first phenomenon to be studied. Since the plasma frequency is ~ 30 MHz, plasma wave phenomena could be studied, even if the confinement time was as short as 100 μs.

Table 5.2. Design parameters of an electron–positron experiment using a combined Penning–Paul trap. [Following reference[44], values here are in cgs (centimeter, gram, seconds), not S. I. units.]

Quantity	Design Value
density (cm–3)	10^7
plasma length (cm)	30
plasma radius (cm)	0.5
electrode inner diameter (cm)	1
particle number	5×10^8
RF frequency (MHz)	200
RF voltage (V rms)	100
rRFpotential well (V)	5
CO_2 pressure (mbar)	1.3×10^{-6}
plasma temperature (eV)	0.5

While this combined trap is suitable for low-density electron–positron plasma studies, it is not likely to be a viable geometry for confining high-density plasmas. This is due to plasma heating, which will increase rapidly with plasma density and the unavailability of a sufficiently rapid cooling mechanism to counteract it. While heating due to Coulomb collisions could be reduced at higher plasma temperatures, Ps formation (cf., Chapter 4) will quickly become a problem.

Magnetic-mirror confinement of hot electron–positron plasmas. Experimental studies of relativistic electron–positron plasmas will be much more challenging. The plasma limit requires $n \lambda_D^3 >> 1$, and $\lambda_D <$ L, where L is the characteristic dimension of the charge cloud. Thus, in

order to have λ_D as small as 0.01 m at T_e > 200 keV (i.e., a mildly relativistic plasma), a density of $n = 10^{18}$ m^3 is required. At least, one must have $L = 10\ \lambda_D$ to study plasma wave phenomena, which in turn requires confining 10^{15} positrons. Beyond the challenge of accumulating such a large number of positrons, their confinement in a neutral plasma is expected to be a great challenge.

One possible geometry for such an experiment is a so-called magnetic mirror.[j] An experiment designed to test this confinement scheme for positrons is shown in Figure 5.19. In this experiment, positrons were accumulated from a 0.6 mCi ^{22}Na source and polycrystalline tungsten moderator.[59] It turns out that confinement in a magnetic mirror is better when the plasma is hot (i.e., thereby reducing the loss due to Coulomb collisions). In the mirror, it is also beneficial to arrange $T_\perp >> T_{||}$, where $T_\perp$ and $T_{||}$ are the perpendicular and parallel temperatures of the particles. Both conditions can be achieved relatively easily for electron-mass particles by heating at the cyclotron frequency using microwave radiation, and this is what was done in the experiment of reference[59]. The result was the confinement of ~ 10^4 positrons with confinement times of ~ 20 s and densities of ~ 5 x 10^8 m^{-3}. Given that the incident slow positron flux was low (~ 500/s), the results of this experiment are encouraging.

Confinement of the positrons can be further increased by placing electrodes on either end of the mirror, biased to as large a potential as possible. In this case, positrons exiting the usual “loss cone" in mirrors (i.e., particles with low values of $E_\perp/E_\parallel$ are not confined by the mirror fields) would be reflected back into the magnetic mirror. One unwanted side effect of the hot plasma is the intense X-ray and gamma-ray cyclotron emission from the hot particles.

---

[j] Particle confinement in a magnetic mirror relies on the fact that, in a slowly varying B-field, $E_\perp/B$ is a constant. Since the B-field does no work, this implies that, as B increases, $E_\parallel$ decreases. Thus, for a sufficiently strong field, particles are reflected (i.e., "mirrored"). See reference[57].

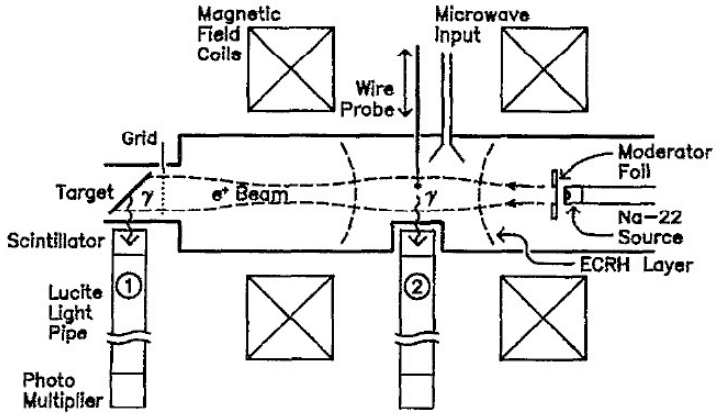

Fig. 5.19. Experimental arrangement to confine positrons in a magnetic mirror using a ^{22}Na source and moderator located in the mirror-field region.[59] In principle, such a configuration could be used to capture fast positrons from the source (i.e., eliminating the need for a moderator). Reprinted from reference[59].

Confinement in a stellarator. One of the simplest possibilities to confine a neutral plasma is to bend the field around into a toroidal (i.e., "donut") shape. However, plasma in a purely toroidal magnetic field is unstable to vertical drifts. In a tokamak, these drifts are mitigated by twisting the magnetic field lines using an induced toroidal current in the plasma. In the stellarator, this twist of the magnetic field is accomplished by external field coils. Both the stellarator and the tokamak were originally developed to confine hot fusion plasmas.[57,60]

The Columbia Non-neutral Torus (CNT), located at Columbia University was built specifically to conduct studies of non-neutral plasmas.[4,61] It has the capability to span the entire range of neutralization from pure electron to quasi-neutral plasmas, with a long-term goal of studying electron–positron plasmas. This device is a two-period, classical stellarator. It has the distinguishing feature, illustrated in Figure 5.20, that the required magnetic topology is created simply by four circular coils. The magnetic surfaces that this device generates are illustrated in Figure 5.21.

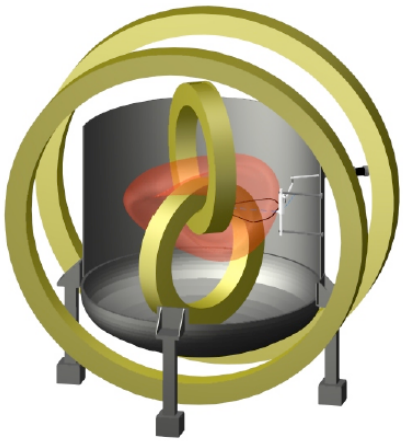

Fig. 5.20. The Columbia Non-neutral Torus plasma device showing a cutaway of the vacuum vessel, the four circular magnetic field coils that produce the stellerator field, and the calculated magnetic surfaces (faint deformed donut). For spatial scale, the vacuum vessel is approximately 1.8 m in diameter. Drawing courtesy of T. S. Pedersen.

This device is capable of confining stable, small-Debye-length plasmas with relatively long confinement times. Basic confinement and transport in the device are now broadly understood. Recently, a flux-surface-conforming electrostatic boundary mesh has been incorporated into the device. With this improvement, confinement times for pure electron plasmas are ~ 0.3 s. The design parameters for an electron–positron experiment in the CNT are a plasma volume of 0.1 m^3, T = 4 eV, n = 3 x 10^{12} m^{-3} and λ_D = 1 cm, with similar electron and positron inventories of ~ 10^{12} particles per species.

In 2012, a collaboration was formed to conduct such an electron–positron plasma experiment. It involves T. S. Pedersen and collaborators, who are now at the Max Planck Institute for Plasma Physics, Greifswald, Germany, Christoph Hugenschmidt and collaborators at the Munich FRM–II Research Reactor, and the UCSD positron group.[62] As described in reference[62], the experiment will be done using a new and more compact superconducting stellerator. The source of positrons will be the NEPOMUC facility (i.e., neutron induced positron source, Munich).

.

Fig. 5.21. The magnetic field topology in the CNT stellarator. Field lines on each of the (colored) surfaces remain on that surface as they transit both the long way and short way around the device. It is this twist of the field lines, which are induced by the external field coils shown in Figure 5.21, that stabilizes the confined plasma. Drawing courtesy of T. S. Pedersen.

5.5. Concluding Remarks

A method was described to extract beams of tailored width and brightness in a non-destructive, reproducible manner from plasmas in a PM trap. Simple analytical formulae predict the beam width and energy spread; key parameters of interest for a range of applications. The ability to extract multiple, nearly identical beams was demonstrated, utilizing over 50 % of a single trapped plasma with no loss of particles. Finally, a scenario was discussed in which the techniques described here can be used to produce high-quality electrostatic beams that are expected to be useful for a variety of positron applications. One major result of this work will likely be the ability to extract such beams from cryogenic plasmas. While challenging, this will offer the possibility of creating a new generation of bright, cold positron-beam sources with considerable potential for new physics and technology.

In a second area, key steps were described in the development of an MCT for the storage of large numbers of positrons. The availability of such large numbers of positrons opens up many new possibilities, providing bursts of positrons far larger than are available by any other means. The short-term goal of a trap for 10^{12} positrons is likely conservative, and we believe that it has a high probability of success. In the present design, this MCT could be made to fit in a volume of only a few cubic meters. It calls for a superconducting magnet and cryogens or a refrigerator. However, one can expect a rapid learning curve associated with the underlying science and technology. It is likely that further improvements in design can be made early in the development of such a multicell device, including increases in storage capacity and confinement time, decreases in the weight and size, and the reduction of other logistical requirements.

The third topic discussed here was the development of methods to study electron–positron plasmas. There are several possibilities in this area, each with advantages for specific kinds of studies. While it is fairly clear that such studies can be conducted, it is unclear what will be the optimum approach. One early focus will likely be study of the transition from single-component plasma confinement, to that in a partially compensated plasma, to that in a neutral plasma. The mechanisms of outward plasma transport in the three cases may well be quite different and interesting. Another topic, while challenging, is study of relativistic pair plasmas. It offers tremendous opportunities to make contact with the many theoretical studies that have been conducted to date.

There are presently world-class positron sources at the nuclear reactors at North Carolina State University[63] and in Munich, Germany[64] that could serve as sources for an electron–positron plasma experiment in a stellarator of the CNT design. Another strong source is being developed at the University of California Riverside.[65] These devices are, or will be, capable of slow positron fluxes ~ 5 x 10^8 – 10^9 e^+/s, and further increases in source strengths are under development. These intense positron sources would be ideal to fill an MCT. Further, they would be excellent for electron–positron experiments such as those described above. In this case, the MCT would be used to accumulate

sufficient numbers of positrons (e.g., $N_{tot} \sim 10^{11} - 10^{12}$) from a strong source, which would then be injected in bursts into the CNT in times ~ 10 ms.

Not addressed here, but extremely interesting, is the desire to develop methods to provide ultra-intense, bright bursts of positrons for applications such as creating a Ps Bose–Einstein condensate (BEC), and eventually, an annihilation gamma-ray laser. The MCT can likely be dumped in tens of milliseconds, but much shorter bursts are desirable for the Ps BEC and other applications. It is likely that achieving these goals will be enabled by better general understanding and control of single-component antimatter plasmas.

At a more general level, the research thrusts discussed here provide examples of the potential of non-neutral plasma physics to impact upon antimatter physics.

Acknowledgments

We thank T. S. Pedersen for the material on the Columbia Non-neutral Torus, M. Bajpai for helpful discussions regarding an electron-positron plasma experiment, E. A. Jerzewski for his expert technical assistance in the experiments at UCSD, and M. Charlton for his careful reading of the manuscript and helpful suggestions. This work is supported by the U. S. DOE/NSF Plasma Initiative.

References

1. C.M. Surko, "Accumulation, Storage and Manipulation of Large Numbers of Positrons in Traps I. – The Basics" in Knoop, M., Madsen, N. and Thompson, R. C. (eds), *Physics with Trapped Charged Particles* (Imperial College Press, London, 2013) pp. WWW – ZZZ.
2. C. M. Surko, G. F. Gribakin and S. J. Buckman, Low-energy positron interactions with atoms and molecules, *J. Phys. B: At. Mol. Opt. Phys.* **38**, R57–R126 (2005).
3. R. G. Greaves, J. M. Moxom, Recent results on trap-based positron beams, *Mat. Sci. Forum* **445–446**, 419–423 (2004).
4. T. S. Pedersen, A. H. Boozer, W. Dorland, J. P. Kremer and R. Schmitt, Prospects for the creation of positron–electron plasmas in a non–neutral stellarator, *J. Phys. B: At. Mol. Opt.* **36**, 1029–1039 (2003).

5. C. M. Surko and R. G. Greaves, Emerging science and technology of antimatter plasmas and trap-based beams, *Phys. Plasmas* **11**, 2333–2348 (2004).
6. J. R. Danielson, T. R. Weber and C. M. Surko, Extraction of Small–diameter Beams from Single-component Plasmas, *Appl. Phys. Lett.* **90**, 081503–081503 (2007).
7. T. R. Weber, J. R. Danielson and C. M. Surko, Creation of Finely Focused Particle Beams from Single-Component Plasmas, *Phys. Plasmas* **15**, 012106–012110 (2008).
8. T. R. Weber, J. R. Danielson and C. M. Surko, Energy Spectra of Tailored Particle Beams from Trapped Single-component Plasmas, *Phys. Plasmas* **16**, 057105–057108 (2009).
9. B. R. Beck, J. Fajans and J. H. Malmberg, Temperature and anisotropic-temperature relaxation measurements in cold, pure-electron plasmas, *Phys. Plasmas* **3**, 1250–1258 (1996).
10. D. H. E. Dubin, Collisional Transport in Nonneutral Plasmas, *Phys. Plasmas* **5**, 1688 (1998).
11. J. R. Danielson and C. M. Surko, Radial Compression and Torque-balanced Steady States of Single-Component Plasmas in Penning–Malmberg traps, *Phys. Plasmas* **13**, 055706–055710 (2006).
12. D. L. Eggleston, C. F. Driscoll, B. R. Beck, A. W. Hyatt and J. H. Malmberg, Parallel energy analyzer for pure electron plasma devices, *Phys. Fluids B* **4**, 3432–3439 (1992).
13. T. R. Weber, J. R. Danielson and C. M. Surko, Electrostatic Beams from Tailored Plasmas in a Penning–Malmberg Trap, *Phys. Plasmas* **17**, 123507–123510 (2010).
14. A. P. Mills, Brightness enhancement of slow positron beams, *Appl. Phys.* **23**, 189 (1980).
15. C. H. Tseng and G. Gabrielse, Portable trap carries particles 5000 kilometers, *Hyperfine Inter.* **76**, 381–386 (1993).
16. R. A. Lewis, G. A. Smith and S. D. Howe, Antiproton portable traps and medical applications, *Hyperfine Inter.* **109**, 155–164 (1997).
17. C. M. Surko and R. G. Greaves, A multi-cell trap to confine large numbers of positrons, *Rad. Chem. and Phys.* **68**, 419–425 (2003).
18. J. R. Danielson, T. R. Weber and C. M. Surko, Plasma Manipulation Techniques for Positron Storage, *Phys. Plasmas* **13**, 123502–123510 (2006).
19. O. J. Orient, A. Chutjian and V. Garkanian, Minature, high-resolution quadrupole mass-spectrometer array, *Rev. Sci. Instrum.* **68**, 1393–1397 (1997).
20. E. R. Badman and R. G. Cooks, Parallel minature cylindrical ion trap array, *Analytical Chem.* **72**, 3291–3297 (2000).
21. L. V. Jørgensen, M. Amoretti, G. Bonomi, P. D. Bowe, C. Canali, C. Carraro, C. L. Cesar, M. Charlton, M. Doser, A. Fontana, M. C. Fujiwara, R. Funakoshi, P. Genova, J. S. Hangst, R. S. Hayano, A. Kellerbauer, V. Lagomarsino, R. Landua, E. L. Rizzini, M. Macrì, N. Madsen, D. Mitchard, P. Montagna, A. Rotondi, G. Testera, A. Variola, L. Venturelli, D. P. v. d. Werf and Y. Yamazaki, New Source of Dense, Cryogenic Positron Plasmas, *Phys. Rev. Lett.* **95**, 025002–025005 (2005).

22. R. G. Greaves and C. M. Surko, Antimatter plasmas and antihydrogen, *Phys. Plasmas* **4**, 1528–1543 (1997).
23. C. M. Surko and T. J. Murphy, Use of the positron as a plasma particle, *Phys. Fluids B* **2**, 1372–1375 (1990).
24. E. M. Hollmann, F. Anderegg and C. F. Driscoll, Confinement and Manipulation of Non-neutral Plasmas Using Rotating Wall Electric Fields, *Phys. Plasmas* **7**, 2776–2789 (2000).
25. R. G. Greaves, M. D. Tinkle and C. M. Surko, Creation and uses of positron plasmas, *Phys. Plasmas* **1**, 1439–1446 (1994).
26. C. M. Surko, R. G. Greaves and M. Charlton, Stored positrons for antihydrogen production, *Hyperfine Inter.* **109**, 181–188 (1997).
27. C. Hugenschmidt, K. Schreckenbach, M. Stadlbauer and B. Straßer, First positron experiments at NEPOMUC, *Appl. Surf. Sci.* **252**, 3098–3105 (2006).
28. R. Krause-Rehberg, S. Sachert, G. Brauer, A. Rogov and K. Noack, EPOS – an intense positron beam project at the ELBE radiation source in Rossendorf, *Appl. Surf. Sci.* **252**, 3106–3110 (2006).
29. H. M. Chen, Y. C. Jean, C. D. Jonah, S. Chemerisov, A. F. Wagner, D. M. Schrader and A. W. Hunt, Intense slow positron production at the 15 MeV LINAC at Argonne National Laboratory, *Appl. Surf. Sci.* **252**, 3159–3165 (2006).
30. B. R. Beck, J. Fajans and J. H. Malmberg, Measurement of collisional anisotropic temperature relaxation in a strongly magnetized pure electron plasma, *Phys. Rev. Lett.* **68**, 317–320 (1992).
31. R. C. Davidson, *Physics of Nonneutral Plasmas* (Addison-Wesley, Reading, MA, 1990).
32. K. S. Fine, C. F. Driscoll and J. H. Malmberg, Measurements of a nonlinear diocotron mode in pure electron plasmas, *Phys. Rev. Lett.* **63**, 2232–2234 (1989).
33. J. Fajans, E. Gilson and L. Friedland, Autoresonant excitation of the diocotron mode in non-neutral plasmas, *Phys. Rev. Lett.* **82**, 4444–4447 (1999).
34. J. Fajans, E. Gilson and L. Friedland, Autoresonant excitation of a collective nonlinear mode, *Phys. Plasmas* **6**, 4497–4503 (1999).
35. J. Fajans, E. Gilson and L. Friedland, The effect of Damping on Autoresonant (nonstationary) Excitation, *Phys. Plasmas* **8**, 423 (2001).
36. J. R. Danielson and C. M. Surko, Torque-balanced high-density steady states of single component plasmas, *Phys. Rev. Lett.* **95**, 035001–035004 (2005).
37. M. A. Akhalkatsi and G. Z. Machabeli, Generation of Electromagnetic Waves in the Electron–Positron Plasma in the Vicinity of a Pulsar, *Astrophys.* **43**, 282–288 (2000).
38. U. A. Mofiz, Linear modes in the rotating neutron star polar-cap electron–positron plasma, *Phys. Rev. E* **55**, 5894–5900 (1997).
39. J. Zhao, J. I. Sakai, K. I. Nishikawa and T. Neubert, Relativistic particle acceleration in an electron–positron plasma with a relativistic electron beam, *Phys. Plasmas* **1**, 4114–4119 (1994).
40. J. Sakai, M. Eda and W. Shiratori, Wave generation and particle acceleration in an electron–positron plasma, *Phys. Scr.* **T75**, 67–71 (1998).

41. D. Gyobu, J. Sakai, M. Eda, T. Neubert and M. Nambu, Emission of electromagnetic waves from Langmuir waves generated by electron beam instabilities in pair plasmas, *J. Phys. Soc. Japan* **68**, 471–477 (1999).
42. A. D. Rogava, S. M. Mahajan and V. I. Berezhiani, Velocity shear generated Alfven waves in electron–positron plasmas, *Phys. Plasmas* **3**, 3545–3555 (1996).
43. T. Kitanishi, J. Sakai, K. Nishikawa and J. Zhao, Electromagnetic waves emitted from an electron–positron plasma cloud moving across a magnetic field, *Phys. Rev. E* **53**, 6376–6381 (1996).
44. R. G. Greaves and C. M. Surko, "Practical Limits on Positron Accumulation and the Creation of Electron-Positron Plasmas", in Anderegg, F., Schweikhard, L. and Driscoll, C. (eds), *Non-Neutral Plasma Physics IV* (American Institute of Physics, Melville, NY, 2002), pp. 10–23.
45. V. Tsytovich and C. B. Wharton, Laboratory electron–positron plasma-a new research object, *Comments Plasma Phys. Controlled Fusion* **4**, 91–100 (1978).
46. R. G. Greaves and C. M. Surko, An electron–positron beam-plasma experiment, *Phys. Rev. Lett.* **75**, 3846–3849 (1995).
47. S. J. Gilbert, D. H. E. Dubin, R. G. Greaves and C. M. Surko, An electron–positron beam-plasma instability, *Phys. Plasmas* **8**, 4982–4994 (2001).
48. H. Boehmer, Formation of electron–positron plasmas in the laboratory, *AIP Conference Proceedings* **303**, 422–434 (1994).
49. C. Hugenschmidt, Private communication, 2003.
50. D. Umstadter, Review of physics and applications of relativistic plasmas driven by ultra-intense lasers, *Phys. Plasmas* **8**, 1774–1785 (2001).
51. E. P. Liang, S. C. Wilks and M. Tabak, Pair production by ultraintense lasers, *Phys. Rev. Lett.* **81**, 4887–4890 (1998).
52. C. Gahn, G. D. Tsakiris, G. Pretzler, K. J. Witte, P. Thorolf, D. Habs, C. Delfin and C. G. Wahlström, Generation of MeV electrons and positrons with femtosecond pulses from a table-top lasesr system, *Phys. Plasmas* **9**, 987–999 (2002).
53. T. E. Cowan, M. Roth, J. Johnson, C. Brown, M. Christl, W. Fountain, S. Hatchett, E. A. Henry, A. W. Hunt, M. H. Key and A. MacKinnon, Intense electron and proton beams from Peta Watt laser-matter interactions, *Nucl. Instrum. Meth. Phys. Res. A* **455**, 130–139 (2000).
54. P. Zhang, N. Saleh, S. Chen, Z. Shen and D. Umstadter, An optical trap for relativistic plasma, *Phys. Plasmas* **10**, 2093–2099 (2003).
55. H. Chen, S. C. Wilks, J. D. Bonlie, E. P. Liang, J. Myatt, D. F. Price, D. D. Meyerhofer and P. Beiersdorfer, Relativistic Positron Creation Using Ultraintense Short Pulse Lasers, *Phys. Rev. Lett.* **102**, 105001–105004 (2009).
56. J. Myatt, J. A. Delettrez, A. V. Maximov, D. D. Meyerhofer, R. W. Short, C. Stoeckl and M. Storm, Optimizing electron–positron production on kilojoule-class high-intensity lasers for pair-plasma creation, *Phys. Rev. E* **79**, 066409–066410 (2009).
57. F. F. Chen, *Introduction to Plasma Physics and Controlled Fusion, Volume I: Plasma Physics*, Second edition (Springer, New York, 1984).
58. J. Walz, C. Zimmermann and L. Ricc, Combined trap with the potential for antihydrogen production, *Phys. Rev. Lett.* **75**, 3257–3260 (1995).

59. H. Boehmer, M. Adams and N. Rynn, Positron trapping in a magnetic mirror configuration, *Phys. Plasmas* **2**, 4369–4371 (1995).
60. N. A. Krall and A. W. Trivelpiece, *Principles of Plasma Physics* (San Francisco Press, San Francisco, 1986).
61. T. S. Pedersen, J. P. Kremer, R. G. Lefrancois, Q. Marksteiner, X. Sarasola and N. Ahmad, Experimental demonstration of a compact stellarator magnetic trap using four circular coils, *Phys. Plasmas* **13**, 102502–102506 (2006).
62. T. S. Pedersen, J. R. Danielson, C. Hugenschmidt, G. Marx, X. Sarasola, F. Schaue, L. Schweikhard, C. M. Surko and E. Winkler, Plans for the creation and studies of electron–positron plasmas in a stellarator, *New J. Phys.* **14**, 035010–035013 (2012).
63. A. G. Hathaway, M. Skalsey, W. E. Frieze, R. S. Vallery and D. W. Gidley, Implementation of a Prototype Slow Positronium Beam at the North Carolina State University PULSTAR Reactor, *Nucl. Instrum. Meth. in Phys. Res. A* **579**, 538–541 (2007).
64. C. Hugenschmidt, G. Kogel, R. Repper, K. Schreckenbach, P. Sperr, B. Strasser and W. Triftshauser, "NEPOMUC – the new positron beam facility at FRM II" in Hyodo, T., Kobayashi, Y., Nagasima, Y. and Saito, H., (eds), *Proceedings of the International Conference on Positron Annihilation, Volume 445–446* (Materials Science Forum, 2004) pp. 480–482.
65. D. B. Cassidy, R. G. Greaves, S. H. M. Deng, N. Lopez–Valdez, V. Meligne and A. P. Mills, "Development and Applications of an Accelerator Based Positron Source" in Mcdaniel, F. D. and Doyle, B. L. (eds.), *20th International Conference on Applications of Accelerators in Research and Industry* (AIP Conference Proceedings #1099, Toronto CA, 2009), pp. 866–869.